AFRL-AFOSR-VA-TR-2020-0071

Representing and Transforming Sensory Stimuli using Spike Trains

Arunava Banerjee
UNIVERSITY OF FLORIDA

05/19/2020
Final Report

Air Force Research Laboratory
AF Office Of Scientific Research (AFOSR)/ RTB2
Arlington, Virginia 22203
Air Force Materiel Command

REPORT DOCUMENTATION PAGE

Form Approved
OMB No. 0704-0188

1. REPORT DATE *(DD-MM-YYYY)*	2. REPORT TYPE	3. DATES COVERED *(From - To)*
22-06-2020	Final Performance	01 Mar 2016 to 29 Feb 2020

4. TITLE AND SUBTITLE
Representing and Transforming Sensory Stimuli using Spike Trains

5a. CONTRACT NUMBER

5b. GRANT NUMBER
FA9550-16-1-0135

5c. PROGRAM ELEMENT NUMBER
61102F

6. AUTHOR(S)
Arunava Banerjee

5d. PROJECT NUMBER

5e. TASK NUMBER

5f. WORK UNIT NUMBER

7. PERFORMING ORGANIZATION NAME(S) AND ADDRESS(ES)
UNIVERSITY OF FLORIDA
207 GRINTER HALL
GAINESVILLE, FL 32611-5500 US

8. PERFORMING ORGANIZATION REPORT NUMBER

9. SPONSORING/MONITORING AGENCY NAME(S) AND ADDRESS(ES)
AF Office of Scientific Research
875 N. Randolph St. Room 3112
Arlington, VA 22203

10. SPONSOR/MONITOR'S ACRONYM(S)
AFRL/AFOSR RTB2

11. SPONSOR/MONITOR'S REPORT NUMBER(S)
AFRL-AFOSR-VA-TR-2020-0071

12. DISTRIBUTION/AVAILABILITY STATEMENT
A DISTRIBUTION UNLIMITED: PB Public Release

13. SUPPLEMENTARY NOTES

14. ABSTRACT

This final report summarizes the results from the four (3+1 NCE) years of support under the grant. Technical advances were made in three interrelated research areas, with novel optimization frameworks conferring the common theme. (1) An optimization framework that tunes the dynamics of a network of non-spiking neurons to display an observed behavior, was developed. The framework was then used to identify synaptic profiles in a parsimonious network model of the elementary motion detector. To our knowledge, this is the first conductance based compartmental model neuronal network implementation replicating the behavior of the T4 neuron in the fly optic lobe. (2) A framework was developed for the coding and decoding of continuous time signals using an ensemble of spike trains. The technique distinguishes itself in the quality of reconstruction achieved under low spike rate regimes. (3) A framework named Spike-triggered descent was developed to complement the widely used technique, Spike-triggered average, to characterize the response of a neuron to sensory stimuli. The framework improves upon the model assumption from spikes generated using an inhomogeneous Poisson process to spikes generated using a cumulative spike response model. Superior performance was demonstrated on a Locusta migratoria tympanal nerve dataset. The technique has wide applicability to all neural systems that display low levels of noise.

15. SUBJECT TERMS
spike train, H1 Neurons, sensory stimuli

16. SECURITY CLASSIFICATION OF:			17. LIMITATION OF ABSTRACT	18. NUMBER OF PAGES	19a. NAME OF RESPONSIBLE PERSON
a. REPORT	b. ABSTRACT	c. THIS PAGE			BRADSHAW, PATRICK
Unclassified	Unclassified	Unclassified	UU		19b. TELEPHONE NUMBER *(Include area code)* 703-588-8492

FA9550-16-1-0135 Final Report
02/28/2016 to 02/28/2020
Representing and Transforming Sensory Stimuli Using Spike Trains

Arunava Banerjee
Computer & Information Science & Engineering, University of Florida
arunava@ufl.edu

Submitted to: Dr. Patrick Bradshaw
AFOSR
Human Performance and Biosystems

Abstract

This final report summarizes the results from the four (3+1 NCE) years of support under the grant. Technical advances were made in three interrelated research areas, with novel optimization frameworks conferring the common theme. (1) An optimization framework that tunes the dynamics of a network of non-spiking neurons to display an observed behavior, was developed. The framework was then used to identify synaptic profiles in a parsimonious network model of the elementary motion detector. To our knowledge, this is the first conductance based compartmental model neuronal network implementation replicating the behavior of the T4 neuron in the fly optic lobe. (2) A framework was developed for the coding and decoding of continuous time signals using an ensemble of spike trains. The technique distinguishes itself in the quality of reconstruction achieved under low spike rate regimes. (3) A framework named Spike-triggered descent was developed to complement the widely used technique, Spike-triggered average, to characterize the response of a neuron to sensory stimuli. The framework improves upon the model assumption from spikes generated using an inhomogeneous Poisson process to spikes generated using a cumulative spike response model. Superior performance was

demonstrated on a *Locusta migratoria* tympanal nerve dataset. The technique has wide applicability to all neural systems that display low levels of noise.

1 Introduction

The vast majority of neurons in animal brains communicate with one another using action potentials, also known as spikes. How information is represented and transformed using the spike trains of networks of neurons is one of the central problems in Computational Neuroscience. One of the more popular hypotheses, *rate coding*, posits that continuous time signals are encoded in the rate at which the spikes are generated by the neurons. Although, this might be the case in some regions of the brain in some animals, there is now clear evidence that 'continuous-time signal to spike train' coding can be significantly more sophisticated. For example, [33] have shown that the spike train generated by the H1 neuron in the fly optic lobe represents horizontal ego motion in a very complex manner. Additionally, this spike code has sub-millisecond precision, that is, individual spikes shifted by submilliseconds represent different horizontal motion trajectories.

Noise is intrinsic to all physical systems. However, the magnitude of this noise dictates the tools that ought to be used to study the system. All the work described in this report assumes noise levels that are so small (such as in the H1 neuron) that the system is best analyzed as a deterministic system. In the remainder of this section, we present summary abstracts of the three advances made during the course of this grant. In section 2, we describe these results in more detail, In section 3, we list the graduate students that were partially or fully supported by this grant. In section 4, we list publications that were the result of these efforts.

Summary Abstract 1: We present a general optimization procedure that given a parameterized network of nonspiking conductance based compartmentally modeled neurons, tunes the parameters to elicit a desired network behavior. Armed with this tool, we address the elementary motion detector problem. Central to established theoretical models, the Hassenstein-Reichardt and Barlow-Levick detectors, are delay lines whose outputs from spatially separated locations are prescribed to be nonlinearly integrated with the direct outputs to engender direction selectivity. The neural implementation of the delays—which are substantial as stipulated by interomatidial angles—has remained elusive although there is consensus regarding the neurons that constitute the network. Assisted by the optimization procedure, we identify parameter settings consistent with the connectivity architecture and

physiology of the Drosophila optic lobe, that demonstrates that the requisite delay and the concomitant direction selectivity can emerge from the nonlinear dynamics of small recurrent networks of neurons with simple tonically active synapses. Additionally, although the temporally extended responses of the neurons permit simple synaptic integration of their signals to be sufficient to induce direction selectivity, both preferred direction enhancement and null direction suppression is necessary to abridge the overall response. Finally, the characteristics of the response to drifting sinusoidal gratings are readily explained by the charging-up of the recurrent networks and their low-pass nature.

Summary Abstract 2: In many animal sensory pathways, the transformation from external stimuli to spike trains is essentially deterministic. In this context, a new mathematical framework for coding and reconstruction, based on a biologically plausible model of the spiking neuron, is presented. The framework considers encoding of a signal through spike trains generated by an ensemble of neurons via a standard convolve-then-threshold mechanism. Neurons are distinguished by their convolution kernels and threshold values. Reconstruction is posited as a convex optimization minimizing energy. Formal conditions under which perfect reconstruction of the signal from the spike trains is possible are then identified in this setup. Finally, a stochastic gradient descent mechanism is proposed to achieve these conditions. Simulation experiments are presented to demonstrate the strength and efficacy of the framework.

Summary Abstract 3: The characterization of neural responses to sensory stimuli is a central problem in neuroscience. Spike-triggered average (STA), an influential technique, has been used to extract optimal linear kernels in a variety of animal subjects. However, when the model assumptions are not met, it can lead to misleading and imprecise results. We introduce a technique, called spike-triggered descent (STD), which can be used alone or in conjunction with STA to increase precision and yield success in scenarios where STA fails. STD works by simulating a model neuron that learns to reproduce the observed spike train. Learning is achieved via parameter optimization that relies on a metric induced on the space of spike trains modeled as a novel inner product space. This technique can precisely learn higher order kernels using limited data. Kernels extracted from a *Locusta migratoria* tympanal nerve dataset (`http://crcns.org/data-sets/ia/ia-1`) demonstrate the strength of this approach.

2 Results

We now contextualize each problem with the necessary background, following which we briefly describe the technical result. For more detailed descriptions, we refer the reader to the correspondingly titled articles noted in Section 4.

2.1 An Optimization framework for Nonspiking Neuronal Networks and Aided Discovery of a Parsimonious Model for the Elementary Motion Detector

A major goal of Neuroscience is to understand how the activity of identified neural circuits relate to behavior. Recent advances in (semi)automated reconstruction from EM data and immunolabeling have generated a wealth of information regarding the neural connectivity architecture and polarity of synapses in the brains of model organisms. For example, [48] has released an EM volume of the complete Drosophila brain, parts of which have been reconstructed for neural connectivity. These notable advances have, however, not been followed by the anticipated spate of neural implementation solutions to well characterized high level operations. This discrepancy stems from the fact that the dynamics of a neural circuit is determined not only by connectivity and synaptic polarities, but also by the synaptic gain profiles, information which the current techniques do not reveal at the necessary level of detail. Lacking synaptic profile information, relating circuits to behavior has therefore been difficult.

The observation that network behavior is influenced by synaptic profiles also implies that it is, in principle, possible to infer synaptic profiles from the recorded behavior of a network. Such a data driven approach, where a parameterized model is adapted to the characteristics of a dataset, has been the cornerstone of recent successes in Machine Learning. The general problem in the current context, where a network comprises both spiking and nonspiking neurons, is likely both formally and computationally intractable. However, as we demonstrate here, a more restricted class, that of nonspiking neuronal networks, lends itself to this approach. Specifically, we show that local analysis of the trajectories of the corresponding dynamical system is tractable: in operational terms, given a parameterized network of compartmentally modeled conductance based nonspiking neurons interacting with tonically active synapses, computational optimization can tune the parameters to cause the network's behavior to display desired properties. The optimization procedure developed

is general and applies to a large class of parameters, including synaptic profiles as well as morphological properties of the constituent neurons.

In order to showcase the strength of the optimization driven approach, we have chosen a network whose (a) architecture is conserved across multiple insect species, (b) has been characterized in substantial detail, and (c) has well established theoretical models whose relationship to the neural implementation remains to be reconciled. In resolving this problem, we show that computational optimization of parameterized synaptic profiles to fit a network's behavior can be a potent tool when combined with connectivity and synaptic polarity information.

The elementary motion detector (EMD) in the fly brain is a paradigmatic neural computation that has been the subject of intense investigation over decades [6]. Established theoretical models, the Hassenstein-Reichardt (HR) [23] and the Barlow-Levick (BL) [2] detectors prescribe delay lines, the neural implementation of which has thus far remained elusive. Much is however known about the neural circuits that implement the EMD, that we summarized here.

The compound eyes of flies consist of anatomically identical units, called omatidia, laid out in a hexagonal lattice. Visual information processing begins at the photoreceptors in the omatidium, advancing thereafter through neurons in four retinotopically organized neuropile, the lamina, medulla, lobula, and lobula plate. Broad interest in fly motion vision, stemming from its status as a canonical computation, has led to the accumulation of a wealth of data—particularly with regard to the Drosophila—concerning the connectivity architecture and physiology of the neurons in the repeating modules associated with each omatidium, in the lamina [31, 45] as well as the medulla and lobula [44, 42]. Briefly, axons of photoreceptors R1-R6 innervate lamina monopolar cells (LMC) L1-L3 in the corresponding lamina module. Of the cells identified in the lamina, only the joint silencing of the similarly responding [13] L1 and L2 abolishes direction selectivity [45]. Exiting the lamina, motion information is extracted in parallel pathways with L1 feeding the brightness increment (ON) and L2 feeding the brightness decrement (OFF) circuitry [25]. The connectome of the ON module in the medulla has been elucidated in substantial detail (Fig.6 in [44]). Based on the preponderance of different synaptic contacts, the following core circuit emerges (Fig.1a). The primary targets of L1 are Mi1, Tm3, L5, and C3. L5 drives Mi4, C3 drives Mi9, and Mi4 and Mi9 are reciprocally connected. Lastly, Mi1, Tm3, Mi4, and Mi9 constitute the primary inputs to T4 which is the first cell on the pathway to exhibit direction selectivity. Although Fig.6 in [44] contains additional cells and synaptic contacts, our results demonstrate that this parsimonious

circuit is sufficient to manifest direction selectivity, with Mi1/Tm3 providing the direct input and Mi4/Mi9 providing the delayed input into T4. The narrow receptive field T4 comes in four flavors: T4a-d each tuned to one of four cardinal directions. Whole-cell recordings [4] indicate that all of the noted cells are graded potential neurons, and therefore communicate using tonically active synapses [27]. The connectome of the OFF module exhibits strong parallels [42].

We chose to computationally model the ON pathway because data pertaining to the dimensions of neurites and the polarity of synapses is largely available in this case [44]. The principles we have discovered, however, apply to the OFF pathway as well.

We begin with the standard conductance based compartmental modeling methodology, where each neuron is partitioned into equipotential segments whose terminals are then linked to assemble the network (Fig.1c). Each compartment i is modeled using the differential equation,

$$\tau^i \frac{dV^i}{dt} = (E_l^i - V^i) + 2(V_{in}^i - V^i)\pi^i + 2(V_{out}^i - V^i)\pi^i + (E_{syn}^i - V^i)\rho^i \tag{1}$$

where V^i, V_{in}^i and V_{out}^i denote the time varying membrane potential at the middle and the two terminals of a compartment, and E_l^i, E_{syn}^i denote the constant leak and constant synaptic potentials. Also, $\tau^i = C^i/g_l^i, \pi^i = g_a^i/g_l^i$, and $\rho^i = g_{syn}^i/g_l^i$, where C^i, g_l^i, g_a^i and g_{syn}^i denote the constant capacitance, constant leak, constant axial, and time varying synaptic conductances. The scaling by $(1/g_l^i)$ makes π^i and ρ^i dimensionless quantities, which in turn aid in the interpretability of the equation.

Compartments are linked as mandated by the modeled cellular morphology of the neurons (Fig.1a and c). Each terminal of each compartment satisfied one current balance algebraic constraint: if the terminal corresponding to V_{in}^* of compartment $*$ is linked to the terminals corresponding to V_{out}^i of compartments $i = 1 \ldots m$, then setting $V_{out}^i = V_{in}^*$ for all $i = 1 \ldots m$, we have

$$V_{in}^* = (V^*\pi^* g_l^* + \sum_{i=1}^{m} V^i \pi^i g_l^i)/(\pi^* g_l^* + \sum_{i=1}^{m} \pi^i g_l^i) \tag{2}$$

and likewise, if the terminal corresponding to V_{out}^* of compartment $*$ is linked to the terminals corresponding to V_{in}^i of compartments $i = 1 \ldots m$, then setting $V_{in}^i = V_{out}^*$ for all

$i = 1 \ldots m$, we have

$$V^*_{out} = (V^*\pi^* g^*_l + \sum_{i=1}^{m} V^i \pi^i g^i_l)/(\pi^* g^*_l + \sum_{i=1}^{m} \pi^i g^i_l) \tag{3}$$

The V^i_{in} and V^i_{out} in Eq. 1 can be eliminated by plugging in Eq. 2 and Eq. 3, resulting in a system of ordinary differential equations (ODE) involving only the V^i of each compartment.

What remains is the specification of the model for the time varying relative synaptic conductances $g^i_{syn}/g^i_l = \rho^i$ as a function of the presynaptic potential, i.e., $\rho^i(V_{pre})$, where V_{pre} denotes the V^j of the presynaptic compartment. In our model, $\rho^i(V_{pre})$ is parameterized as a monotonically increasing and saturating function of the instantaneous potential V_{pre} of the appropriate presynaptic compartment:

$$\rho^i(V_{pre}) = \frac{\mu^i}{1 + e^{-(\nu^i V_{pre} + \eta^i)}} \tag{4}$$

where the parameters μ^i, ν^i, and η^i, set to be strictly positive, determine the gain, sensitivity, and baseline relative conductance (Fig.1d). For a fixed connectivity architecture, the entire network is thus specified by the set of parameters $\{\pi^i, g^i_l, \mu^i, \nu^i, \eta^i\}$, with i ranging over the finitely many compartments in the network. The input drive into a network is specified as time varying trajectories of presynaptic potentials at the input synapses of the network. Given initial conditions $V^i(0)$ for all compartments i, the entire differential-algebraic system of equations traces out a trajectory for $V^i(t)$, $V^i_{in}(t)$, $V^i_{out}(t)$, in the high dimensional Euclidean space, $\mathbb{R}^{3n}$, where n is the number of compartments.

We now describe, at a conceptual level, the technical advance we have achieved. For a formal and comprehensive description, we refer the reader to the correspondingly titled article in Section 4. Any compartmentally modeled neural system, feedforward or recurrent, can be parameterized as described above, using finitely many parameters. What we have derived is a *new* set of inhomogeneous ODE's that encapsulate how a trajectory for the $V^i(t)$, $V^i_{in}(t)$, $V^i_{out}(t)$, for all i, would change in the limit, if one were to infinitesimally perturb any of the parameters $\{\pi^i, g^i_l, \mu^i, \nu^i, \eta^i\}$, with i ranging over the finitely many compartments in the network. Armed with this new system of ODE's, one can perform a gradient descent on an error functional that models the discrepancy between the observed and desired trajectories of the potentials. Instead of presenting the framework here, we present the final outcome of optimizing the synapses in the EMD network to display the requisite behavior. This is presented via Figures 1,2, and 3, their self contained captions, and Table 1 that reports the optimized synaptic constants. The figures and table are replicated from the article.

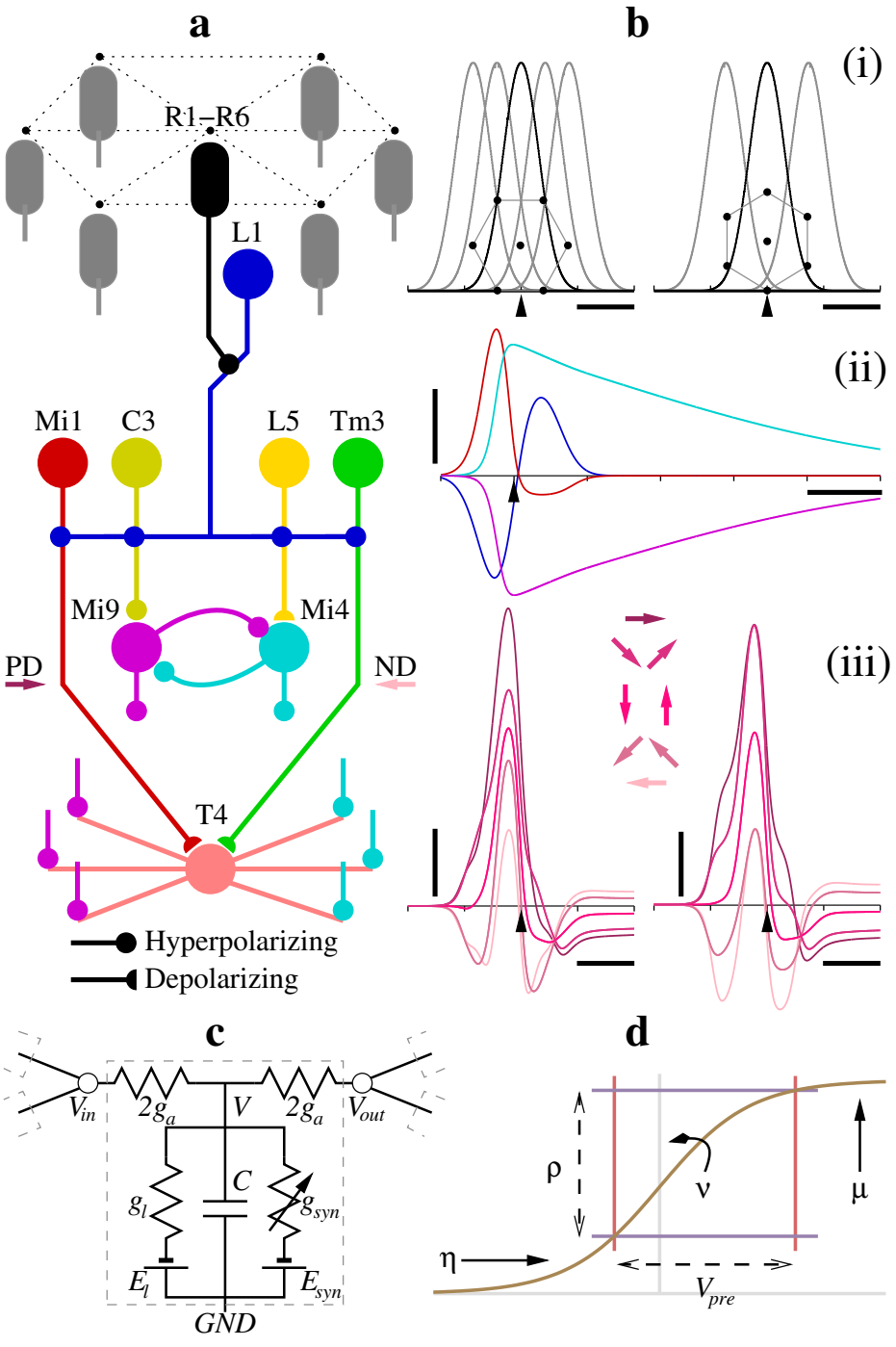

Fig. 1

Figure 1: Neural circuit and representative behavior. a, Circuit for a single module. The circuit is replicated for all modules in the hexagonal lattice, each receiving input from its corresponding photoreceptors (gray). The home module T4 receives input from three Mi9 (from contiguous neighboring modules), three Mi4 (from symmetrically opposing modules), and the Mi1 and Tm3 of the home module. Synaptic parameters, set symmetrically for each Mi4/Mi9 opposing pair, differ for T4s tuned to different cardinal directions (Methods). **b,** Responses of neurons to a 2° wide bar of light traveling at $12°/s$. Responses from circuits tuned to two cardinal directions are shown; responses for the other two cardinal directions are symmetric. (i) Temporal profiles of the normalized stimulus intensity sensed by the photoreceptors of seven contiguous omatidia in the lattice for the two cardinal circuits. Insets display the orientation of the lattice points with respect to the bar stimulus traveling left to right. (ii) Responses of L1, Mi1, Mi4, and Mi9, color coded and shifted along the ordinate by their respective equilibrium resting potentials. The responses of Mi4 and Mi9 are also scaled $\times 10$. (iii) Responses of the home module T4s tuned to the two cardinal directions. Stimulus directions PD, PD$\pm\pi/4$, PD$\pm\pi/2$, ND$\pm\pi/4$, and ND, are with respect to the insets in (i). Horizontal scale bars in (i), (ii), (iii) = $500ms$. Vertical scale bar in (ii) = $5mV$, in (iii) = $1mV$. Pointers on abscissa mark time alignment for the home module. **c,** Conductance based model for a single compartment. Linked compartments i, j satisfy $V^i_{in} = V^j_{out}$. **d,** First model of synapse.

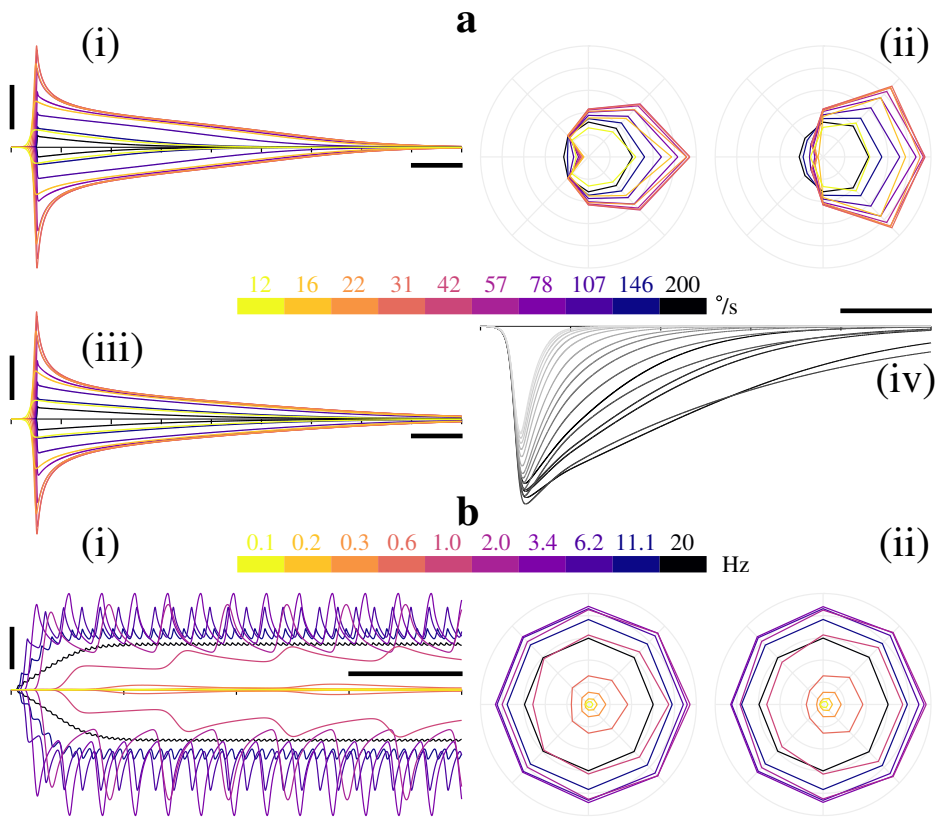

Fig. 2

Figure 2: Responses of Mi4, Mi9, and T4 to bar and drifting sinusoidal grating stimuli. a, Bar stimuli. (i) Responses of Mi4 and Mi9 to a 2° wide bar traveling at different velocities. The responses are color coded and shifted along the ordinate by their respective equilibrium resting potentials. (ii) Corresponding responses of the home module T4s tuned to the two cardinal directions. Peak response above equilibrium resting potential is displayed for each stimulus direction PD, PD$\pm\pi/4$, PD$\pm\pi/2$, ND$\pm\pi/4$, and ND, for the different velocities. (iii) The Mi4-Mi9 dynamics is robust: response of a network with different synaptic parameters (Methods) from another optimization run. (iv) The optimization in action: the delayed and extended dynamics (only Mi9 shown) evolved gradually with changing synaptic parameters for the same stimulus. **b,** Sinusoidal grating stimuli. (i) Responses of Mi4 and Mi9 to a 20° wavelength sinusoidal grating traveling at different velocities. The responses are color coded and shifted along the ordinate by their respective pre-stimulus equilibrium resting potentials. Both the charging-up and the low-pass nature of the circuit are manifest. (ii) Same as a(ii) for this stimuli. Horizontal scale bars in a(i), a(iii), a(iv), b(i) = $1s$. Vertical scale bar in a(i), a(iii) = $2mV$, in b(i) = $3mV$. Voltage increment of concentric circles in a(ii) = $2mV$, in b(ii) = $1mV$.

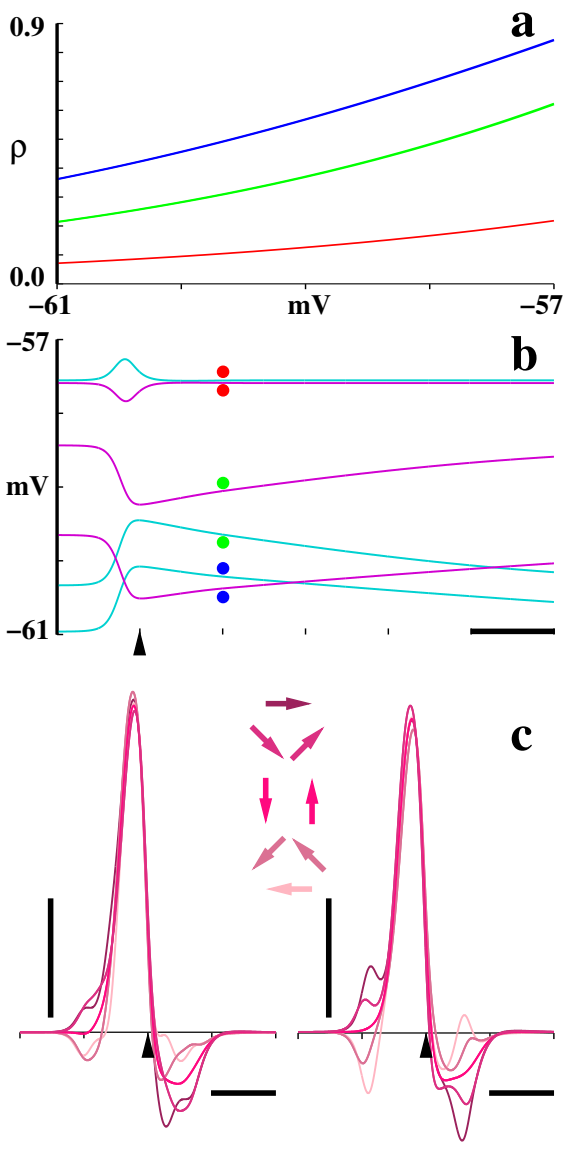

Fig. 3

Figure 3: Pre- and Post Optimized Mi4-Mi9 network and corresponding T4 behavior. a, $\rho(V_{pre})$ of the pair of synapses. Initialization, i.e., pre-optimized synapse pair labeled in red. Optimized synapse pair of the network presented in the article labeled in green. A second optimized pair, corresponding to the network in Fig.2a-iii labeled in blue. Note that the range $[-61, -57]mV$ subsumes the operating range of all three synapse pairs as shown in (b). The optimization was not constrained to update the synapses symmetrically. However, it did to within precision bounds. All parallel graphs of $\rho(V_{pre})$ between the green and blue curves manifest the delay necessary to implement the EMD, demonstrating that the phenomenon is robust. **b,** Responses of Mi4 (cyan) and Mi9 (magenta) in the three networks for a 2° wide bar of light traveling at $12°/s$. Traces are labeled with adjacent color coded dots to distinguish between the three networks. Not only does the optimization delay the time to peak for both Mi4 and Mi9, it also substantially slows the tail decay. Note that both V_{rest} and $V(t)$ change as the synaptic parameters are changed. **c,** Responses of the home module T4s tuned to the two cardinal directions (as in Fig.1b-i) when the Mi4/Mi9 synapses are in the pre-optimized parameter setting in red from (a). Compare these to Fig.1b-iii which corresponds to the Mi4/Mi9 synapses in the post-optimized parameter setting in green from (a). Stimulus directions PD, PD$\pm\pi/4$, PD$\pm\pi/2$, ND$\pm\pi/4$, and ND, are with respect to the insets in Fig.1b-i. Note that directionally selective response is almost absent. Horizontal scale bars in (b), (c), $= 500ms$. Vertical scale bar in (c) $= 1mV$. Pointers on abscissa mark time alignment for the home module as in Fig.1b.

Table 1: Parameters for the full network using $l = 30\mu m$ compartments.

Presynaptic Neuron (Diameter d, Length l)	Postsynaptic Neuron	E_{syn}	μ	ν	η
R1-R6 $(-,-)$	L1	$-85mV$	40.0	3.0	-3.82
L1 $(1\mu m, 100\mu m)$	Mi1/C3/L5	$-85mV$	5.0	0.4	27.4
L5 $(0.6\mu m, 60\mu m)$	Mi4	$0mV$	0.6	0.3	15.0
C3 $(0.6\mu m, 60\mu m)$	Mi9	$-85mV$	0.6	0.3	15.0
Mi4 $(0.6\mu m, 60\mu m)$	Mi9	$-85mV$	4.03555	0.29494	15.10545
Mi9 $(0.6\mu m, 60\mu m)$	Mi4	$-85mV$	4.03574	0.29485	15.10667
Mi1 $(0.6\mu m, 60\mu m)$	T4a(b)	$0mV$	1.5 (1.5)	0.1	7.4912
Mi9 $(0.6\mu m, 60\mu m)$	T4a(b)	$-85mV$	1.5 (2.25)	1.0	58.435
Mi4 $(0.6\mu m, 60\mu m)$	T4a(b)	$-85mV$	1.5 (2.25)	1.0	60.317

2.2 Signal Coding and Perfect Reconstruction using Spike Trains

Spike based encoding of sensory stimuli is a hallmark of biological systems. It is now well-established that the coding of continuous time sensory signals in spike trains is a complex and diverse phenomenon, and is fairly deterministic in many animal sensory pathways[32, 12, 34, 46, 26, 33]. Spike train representations, when sparse, are not only intrinsically energy efficient, but can also facilitate computation at later stages of processing[18, 22]. In their seminal work, Olshausen and Field [35] showed how efficient codes can arise from learning sparse representations of natural stimulus statistics, resulting in striking similarities with observed biological receptive fields. Smith and Lewicki [28, 9] likewise showed that auditory filters could be estimated by training a population spike code model with natural sounds. These studies, by and large, fall under the general framework of dictionary learning: identifying an over-complete dictionary $\{\phi_j | j = 1 \dots m\}$ such that each stimulus s_i in an ensemble $\{s_i | i = 1 \dots n\}$ can be represented as $s_i = \sum_{j=1}^{m} \alpha_j \phi_j$ where the vector of coefficients α_j is sparse. The studies only made passing reference to how the α_j's may be derived (e.g. matching pursuit [29]) or even be represented (e.g. local population of neurons spiking probabilistically proportional to α_j in [9]). Lacking clearly specified plausible neural implementations, the extent to which the proposed schemes underlie biological sensory processing therefore remained unclear. To remedy this, several subsequent learning techniques based on biologically plausible models of spiking neurons have been proposed. For example, [49] developed a biophysically motivated

spiking neural network which for the first time predicted the full diversity of V1 simple cell receptive field shapes when trained on natural images. Elsewhere [41] presented a rate encoded spiking neural network of integrate-and-fire neurons demonstrating convergence to nearly optimal encodings.

Although these results signify substantial progress, the classical signal processing question of what class of signals support perfect or approximate reconstruction when coded using spike trains, remains to be fully resolved. Admittedly, the very coarse $\Sigma\Delta$ quantization of bandlimited signals investigated in [14] does amount to a spike train representation. However, due to the classical nature of its framework, not only is biological plausibility not a concern, but also coding is explored in the oversampled regime. Along similar lines, [11] has explored the spike generating mechanism of the neuron as an oversampling, noise shaping analog-to-digital converter.

Here we present a new framework for coding and reconstruction that begins with a biologically plausible coding mechanism which is a superset of the standard leaky integrate-and-fire mechanism. Reconstruction is first formulated as an optimization that minimizes the energy of the reconstructed signal subject to consistency with the spike train, and then solved in closed form. We then identify a general class of signals for which reconstruction is provably perfect under certain conditions. Surprisingly, the result instantiates a version of Barlow's "efficient coding hypothesis" [3], which posits that the coding strategy of sensory neurons should be adapted to the statistics of the stimuli in an animal's natural environment.

Coding: Formally, we assume the input signal $X(t)$ to be a *bounded continuous function* in the interval $[0, L]$ for some $L \in R^+$, i.e., we are interested in the class of input signals $\mathcal{F} = \{X(t)|X(t) \in C[0, L]\}$. Since the framework involves signal snippets of arbitrary length, this choice of L is without loss of generalization. We assume an ensemble of convolution kernels $K = \{K^j|j \in Z^+, j \leq n\}$, consisting of n kernels $K^j, j = 1, \ldots, n$. We assume that $K^j(t)$ is a continuous function on a bounded time interval $[0, T]$, i.e. $\forall j \in \{1, \ldots, n\}, K^j(t) \in C[0, T]$ for some $T \in R^+$. Finally, we assume that K^j has a time varying threshold denoted by $T^j(t)$.

The ensemble of convolution kernels K encodes a given input signal $X(t)$ into a sequence of spikes $\{(t_i, K^{j_i})\}$, where the i^{th} spike is produced by the j_i^{th} kernel K^{j_i} at time t_i if and only if:

$$\int X(\tau)K^{j_i}(t_i - \tau)d\tau = T^{j_i}(t_i) \tag{5}$$

We assume that the time varying threshold $T^j(t)$ of the jth kernel remains constant at C^j until that kernel produces a spike, at which time an *after-hyperpolarization potential (ahp)*

kicks in to raise the threshold to a high value $M^j \gg C^j$, which then drops back linearly to its original value within a refractory period δ_j. Formally, the threshold function $T^j(t)$ of the j^{th} kernel is given by:

$$T^j(t) = \begin{cases} C^j, & t - \delta_j > t_l^j(t) \\ M^j - \frac{(t - t_l^j(t))(M^j - C^j)}{\delta_j}, & t - \delta_j \leq t_l^j(t) \end{cases} \tag{6}$$

Where $t_l^j(t)$ denotes the time of the last spike generated by K^j prior to time t. Notably, apart from the contribution due to the *ahp*, we have considered the threshold of the j^{th} kernel (alternately called a neuron) to be a constant C^j in our model.

Decoding: The objective of the decoding module is to reconstruct the original signal from the encoded spike trains. Considering the prospect of the invertibility of the coding scheme, we seek a signal that satisfies the same set of constraints as the original signal when generating all spikes apropos the set of kernels in ensemble K. Recognizing that such a signal might not be unique, we choose the reconstructed signal as the one with minimum $L2$-norm. Formally, the reconstruction (denoted by $X^*(t)$) of the input signal $X(t)$ is formulated to be the solution to the optimization problem:

$$\begin{aligned} X^*(t) &= \underset{\tilde{X}}{\operatorname{argmin}} ||\tilde{X}(t)||_2^2 \\ \text{s.t.} &\int \tilde{X}(\tau) K^{j_i}(t_i - \tau) d\tau = T^{j_i}(t_i); 1 \leq i \leq N \end{aligned} \tag{7}$$

where $\{(t_i, K^{j_i}) | i \in \{1, ..., N\}\}$ is the set of all spikes generated by the encoder.

Our work presents several theorems that (a) identify the precise class of signals that can be coded and perfectly reconstructed, and (b) present formal bounds for approximate reconstruction. The work also presents a stochastic gradient descent mechanism to optimize kernels so as to achieve these conditions. For these we refer the reader to the correspondingly titled article.

Here we present results from experiments on an audio dataset that demonstrates the efficacy of the framework. We chose the Freesound Dataset Kaggle 2018 (or FSDKaggle2018 for short), an audio dataset posted on Kaggle referred in [19], containing 18,873 audio files annotated with labels from Google's AudioSet Ontology [20]. For our purpose we ignored the labels and only focused on the sound data itself, since we were only interested in encoding and decoding of input signals. All audio samples in this dataset are provided as uncompressed PCM 16bit, 44.1kHz, mono audio files, with each file consisting of sound snippets of duration ranging between 300ms to 30s. In each trail of our experiment, we reported the accuracy

in reconstruction based on our proposed methodology over at least 1000 randomly chosen sound snippets from the training samples of the dataset. For ease of computation, we kept the length of the input audio snippets to be relatively small (ideally of size less than 5ms). This choice of considering small snippets as input made the computation feasible on limited resource machines within reasonable time bounds. This choice is without loss of generalization and for encoding signals of greater length, reconstruction using this framework can be done piece-wise, partitioning a longer signal into smaller pieces, reconstructing piece-wise and finally stitching the reconstructed pieces together. Results of our experiment are reported by varying the number of kernels, the kernel thresholds or the absolute refractory period.

Bag of Kernels: The proposed encoding technique is operational on a bag of kernels. So we needed to choose a suitable set of kernels for our experiments. Since gammatone filters are widely used as reasonable models for cochlear filters in auditory systems [36] and mathematically, are simple enough to represent, in our experiments for the bag of kernels we chose kernels whose response functions are gammatone filters. The implementation of the filterbank is similar to the one provided in [43], and we have used up to 2000 gammatone kernels whose center frequencies are equally spaced on the ERB scale. Figure 4 shows a sample gammatone filter used as a kernel whose center frequency is at 250 Hz. Rest of the kernels were similar in shape, scaled differently along the time axis based on their corresponding center frequencies.

Results: In each trial of our experiment, the initial threshold value and the absolute refractory period was kept low enough so that for each sound snippet we could get nearly perfect reconstruction at a high spike rate. Figure 5 displays the spikes generated by a subset of the kernels for a representative sound snippet. Once we got a reconstruction at a high spike rate, we discarded less important spikes sequentially to get a compressed representation of each snippet. Figure 6 shows the reconstruction results of a trail with bag of kernels consisting of 2000 gammatone filters over more than 1000 sound snippets chosen from the above mentioned dataset. As one can infer from Figure 6, reconstruction is almost prefect ($\approx 40DB$) at high spike rate ($\approx 15kHz$), and then as we gradually keep discarding spikes based on their importance the reconstruction accuracy goes down. From the results it is clear that based on an application's requirements, a suitable point on the graph can be chosen to get the necessary reconstruction accuracy at a reasonable spike rate.

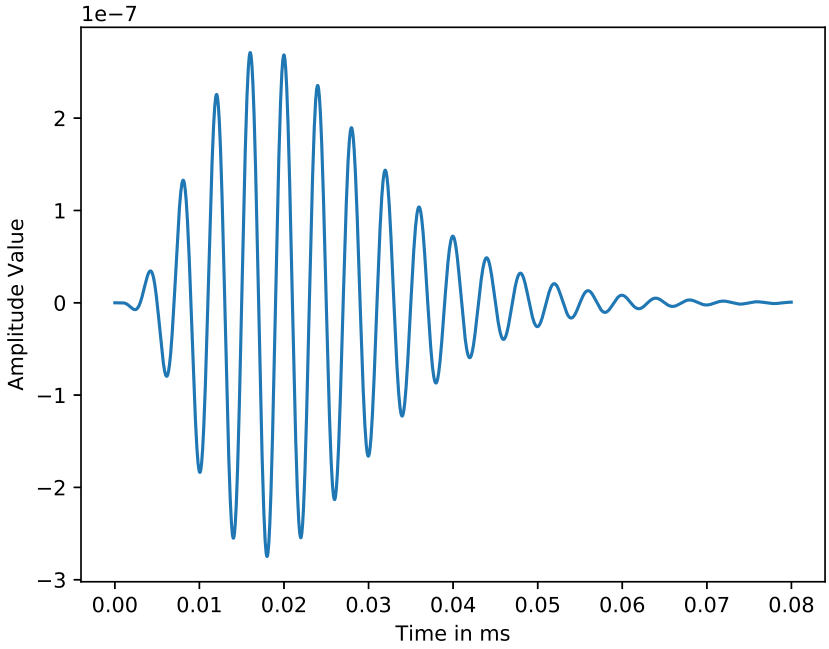

Fig. 4. A sample gammatone filter used as a kernel with center frequency at 250 Hz.

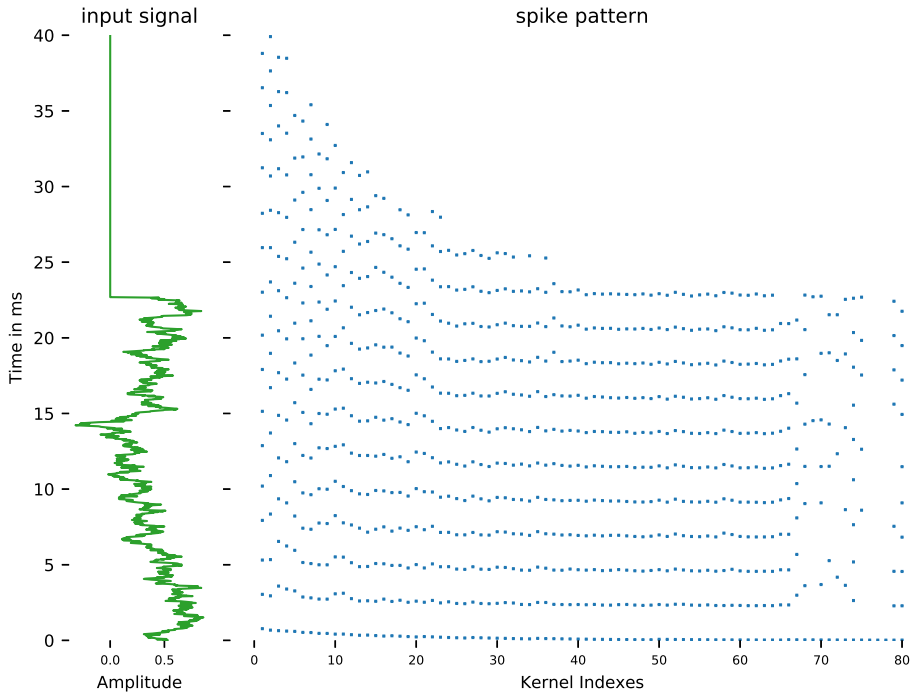

Fig. 5. The spike pattern of 80 chosen kernels from the bag of kernels. On the left the input signal is shown in green and on the right the spike pattern of the chosen 80 kernels is shown on the same time scale.

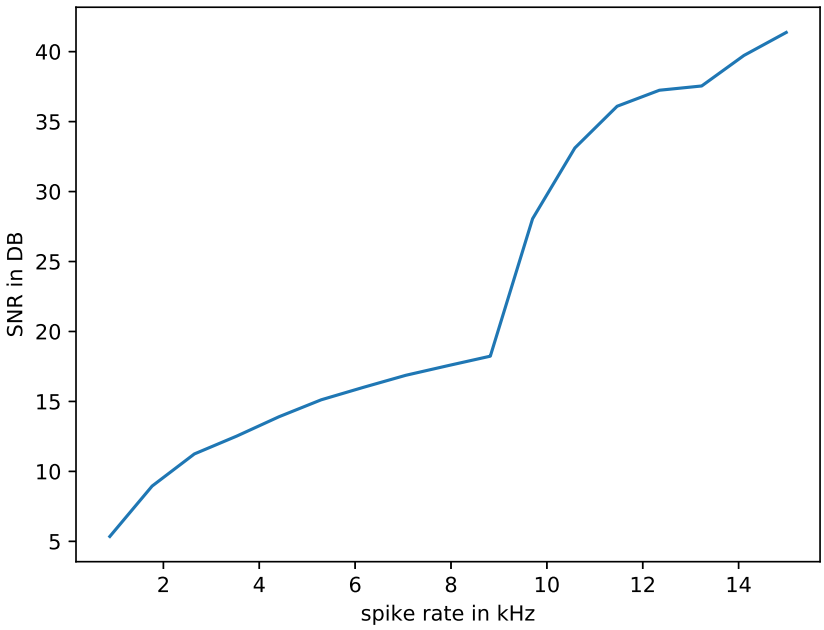

Fig. 6. Plot of SNR values at different spike rates averaged over reconstruction of 1000 sound snippets with a bag of kernels consisting of 2000 gammatone filters

2.3 Spike-Triggered Descent

A major goal of sensory neuroscience is to precisely characterize the mapping that specifies how a neuron responds to sensory stimuli. This response function accounts for intermediary physical processes along with activity of the entire network upstream from the target neuron. The complexity of this problem arises from variations in network connectivity and constituent ion channels which cause wildly differing behavior. There's additional difficulty in a direct component wise analysis resulting from discontinuity of the spiking behavior caused by Hodgkin Huxley ion channels [24]. The inaccessible and innumerable physical parameters create complex interactions which lead to intractable calculations necessitating model simplifications.

A key simplifying assumption comes from signal processing: Any time-invariant continuous nonlinear operator with fading memory can be approximated by a Volterra series operator [7]. The overall impact upon the membrane potential by the upstream network can then be described by a set of Volterra Wiener kernels [47] [5] [37]. Using the first order kernel: Spike-triggered average (STA), a technique which has seen widespread application, assumes a simple probabilistic model of spike generation. When the model assumptions are met, it returns an optimal first order kernel. We introduce a new technique, called spike-triggered descent (STD), which can learn higher order kernels and yield higher accuracy. These techniques approximate the desired kernel by constructing a relationship between sensory stimuli and the spike trains they cause.

Here we give an overview of how STA [15] [30] [10] [40] and STD work, describe their models, and point out a few key differences. STA is based on the linear non-linear Poisson cascade model (LNP) which convolves the signal with a linear kernel, applies a point nonlinearity to convert it into a firing rate, and then samples it using an inhomogeneous Poisson point process to generate spikes. Obtaining the kernel from the signal and resulting spikes requires the signal to be a stationary Gaussian process so that Bussgang's theorem [8] can be applied. In contrast to STA, STD is based on the cumulative spike response model (CSRM) [21] and can approximate higher order kernels for any sufficiently complex signal. Replacing the nonlinear Poisson spike generation, the CSRM spikes occur when the convolution's resulting membrane potential exceeds threshold which inhibits future spikes by way of an after hyperpolarizing potential (AHP). STD works by comparing simulated and recorded spike trains to form a gradient that optimizes kernel parameters.

Neuroscientists use STA because it recovers the optimal linear kernel and is easy to use.

However, the reliance on the stimulus being a Gaussian process and the restriction to first order kernels are weaknesses which STD does not share. The techniques can be used in tandem or STD's initial learning kernel can be randomly guessed. Surprisingly without over fitting, it can precisely approximate while reusing limited data. In the following paragraphs, we introduce a spike train metric used in momentum based stochastic gradient descent (SGD) to update kernels that represent response functions.

The cumulative spike response model (CSRM) [21] can be generalized to include the full Volterra series of kernels (8). These kernels, approximated here by splines, represent the impact on the membrane potential by the stimuli's higher order auto-correlates. Increasing n allows for increased pattern detection capabilities. The AHP function $\eta = -Ae^{(t_l - t_k)/\mu}$ models the refractory period which is a region where spikes are highly unlikely to occur right after firing. In contrast to Poisson sampling, the AHP approach is deterministic and imposes a prior state dependency. A spike is generated when a threshold ($\tilde{\Theta}$) is exceeded by the signal convolved with kernel(s) minus past spikes' AHPs. The n-order kernel K_n is a spline function composed of the n-ary Cartesian product of third order cardinal B-splines B_n. The kernel is incrementally updated by the optimization process. At time $t = t_l^O$ the kernel is $K_{l,n} = \sum_i B_{i,l,n}\beta_{i,l,n}$. The current and prior spike times are t_l^O and t_k^O. The AHP parameter μ modifies the refractory time.

$$\tilde{\Theta} = \sum_{n=1}^{\infty} \int \dots \int K_{l,n}(\tau_1 \dots \tau_n; \beta_{i,l,n}) \prod_i^n x(t_l^O - \tau_i) d\tau_i + \sum_k \eta(t_l^O - t_k^O; \mu) \tag{8}$$

Spike-triggered descent updates parameters based off of the distance between simulated and desired spike trains. To support using the distance (11) from [1] on the GCSRM, it is important to also generalize spike trains and show that they're a subset of a vector space with an inner product $\langle \cdot, \cdot \rangle$. Considering augmented spike trains with countably infinite ($\mathbb{N} = \{1, 2, ...\}$) spikes gives the framework the versatility to compare spike trains of any length. The augmentation turns spike trains into tuples of times and coefficients $\boldsymbol{t} = \{(t_i, \alpha_i)\}$. This forms a vector space and provides the foundation for creating an inner product (9) that induces a metric (Methods). Setting the $\alpha' s$ to 1 for finitely many spikes reduces to the usual space of spike trains within a bounded past. This is a subset of the generalization with the same metric and is squared to simplify the algebra (10).

$$\langle \boldsymbol{t^A}, \boldsymbol{t^B} \rangle = \sum_{i,j=1}^{\infty} (\alpha_i^A \times \alpha_j^B) \frac{t_i^A \times t_j^B}{(t_i^A + t_j^B)^2} e^{-\frac{t_i^A + t_j^B}{\tau}} \tag{9}$$

$$E = d^2 = \langle \boldsymbol{t^D} - \boldsymbol{t^O}, \boldsymbol{t^D} - \boldsymbol{t^O} \rangle \tag{10}$$

Setting α values to 1 for N, M spikes, and 0 otherwise, we get:

$$\begin{aligned} E(\boldsymbol{t^D}, \boldsymbol{t^O}) = & \sum_{i,j=1}^{M,M} \frac{t_i^D \times t_j^D}{(t_i^D + t_j^D)^2} e^{-\frac{t_i^D + t_j^D}{\tau}} \\ & + \sum_{i,j=1}^{N,N} \frac{t_i^O \times t_j^O}{(t_i^O + t_j^O)^2} e^{-\frac{t_i^O + t_j^O}{\tau}} \\ & - 2 \sum_{i,j=1}^{M,N} \frac{t_i^D \times t_j^O}{(t_i^D + t_j^O)^2} e^{-\frac{t_i^D + t_j^O}{\tau}} \end{aligned} \tag{11}$$

The gradient descent equations that are used to incrementally reduce the error E can be found in the article. Here we present results from learning the kernel from a recorded dataset that demonstrates the strength of STD.

Sensory neurons which, when given the same stimuli, reliably produce similar spike trains are good candidates to test STD. One such possibility is the tympanal nerve's auditory receptor axons in the *Locusta migratoria* grasshopper whose action potentials, recorded intracellularly, can have a $0.15ms$[39] inter trial jitter. This dataset, collected by Ariel Rokem[17] [16] at the lab of Andreas Herz, was graciously shared through the CRCNS program (http://crcns.org) [38]. The stimuli consisted of a carrier wave perturbed by random amplitude modulations and a cutoff frequency of up to $800Hz$. We used a particular subset of this dataset to demonstrate kernel extraction.

Repeated updates lead to a kernel which attempts to reconstruct the provided spike train. When running a simulation with a known desired neuron the absolute distance between kernels can be measured. In absence of a known answer, and in lieu of a universally accepted metric, we revert to demonstrating the effectiveness by showcasing the simulated spike train reconstruction for a particular kernel. Figure 7 demonstrates this using a (stimuli, spike train) pair as input. The stimuli we used had a cutoff frequency of $200Hz$. The reconstruction (green dashes) was learned from (blue dashes) one of the 6 recorded spike trains for a particular cell ("./crcns-ia1/Data1/03-04-23-ad/"). The reconstruction occasionally fires where the desired does not but the other (orange dashes) recordings do. This is an indication that the underlying model is being accurately represented.

Given that the data set was recorded at $0.05ms$ and borrowing inspiration from Nemenman's work[33], showing that a blowfly's H1 neuron represents information with sub-millisecond precision even for slow stimuli, finer time resolution STD kernels were explored. The best observed reconstruction was for an STD kernel (green) composed of 50 splines and four $0.25ms$ units per knot interval shown in Figure 8 along with raw (blue) and smoothed (orange) STA kernels. The STA results were omitted from Figure 7 due to a large variety of low quality reconstructions. It was trained with all 6 recorded spike trains, different sized kernels, various levels of smoothing, and multiple spike generation methods (LNP, CSRM). STD is a better technique for learning kernels that have the ability to reconstruct spike trains.

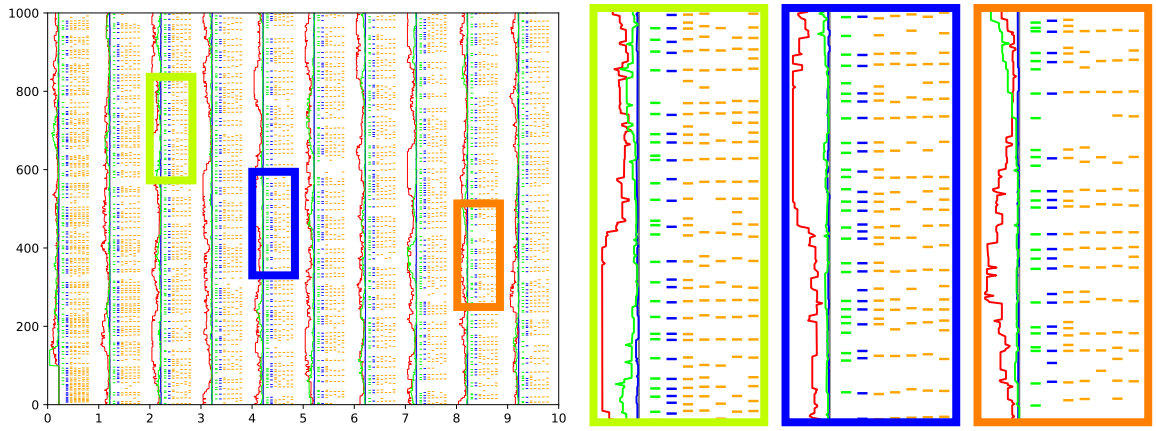

Fig. 7. **a**, The *Locusta migratoria* spike data (blue and orange dots) collected by A. Rokem in cell "./crcns-ia1/Data1/03-04-23-ad/" corresponding to the "gauss_st6_co200.dat" stimuli with a cutoff frequency of $200Hz$. The recording is sliced up with milliseconds on the y axis and seconds on the x for a total of 10 seconds. Each spike train consists of approximately 1000 spikes. The goal was to train an STD kernel that could reconstruct (green dashes) the desired (blue dashes) spike train. There are 5 other recordings (orange dashes) for this stimuli and cell. The final kernel's simulated spike train closely approximates the desired. The green line represents error between the learning and desired spike trains from a preceding window of $100ms$ and is clipped to a range from 0 to 6. Similarly, the blue and red lines represent the minimum and maximum error between any pair of recorded spike trains. **b**, Zoomed sections of the reconstruction were randomly chosen. Notice that the learning error is often between the minimum and maximum errors between recordings. Additionally, a simulated spike will sometimes align with the other recordings even when the desired does not. These are indications that the kernel accurately represents underlying model.

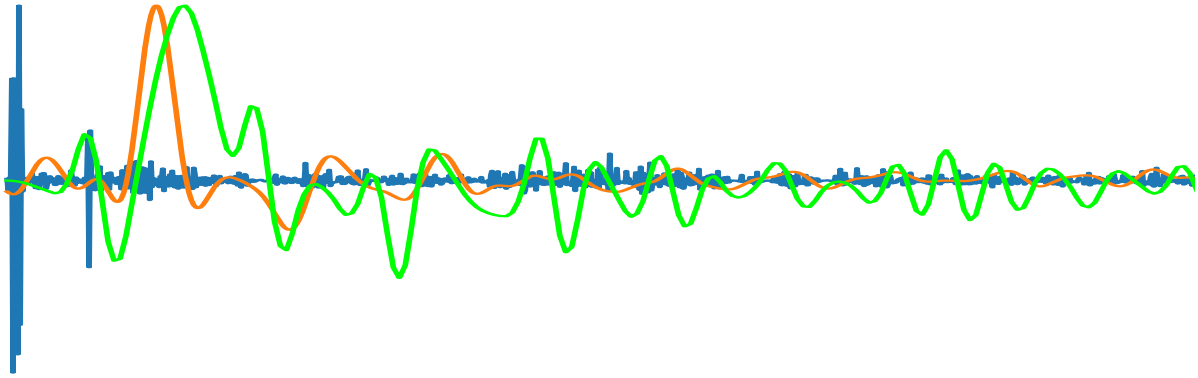

Fig. 8. The raw STA kernel (blue) spanning 1000 time units of $0.05ms$ was smoothed (orange) and compared with the STD result (green). The smoothed STA kernel was the result of of convolving 5 times against a box spline spanning $1ms$.

3 Personnel

The following is a list of individuals who have worked on research supported in whole or in part by the Air Force Office of Scientific Research under Grant FA9550-16-1-0135.

- (PI) Arunava Banerjee, Computer and Information Science and Engineering, University of Florida
- Gokhan Kaya, graduate student (Ph.D completed)
- Tae Seung Kang, graduate student (Ph.D completed)
- Inchul Choi, graduate student (Ph.D completed)
- Fardad Jalili Talchegah, graduate student (M.S. completed)
- Michael Kummer, graduate student (Ph.D in progress)
- Anik Chattopadhyay, graduate student (Ph.D in progress)

4 Publications

The publications listed below represent papers, archived preprints under review, and theses supported in whole or in part by the Air Force Office of Scientific Research under Grant FA9550-16-1-0135.

1. Gokhan Kaya, Arunava Banerjee, (2017) Signal Coding and Reconstruction Using Deterministic Spiking Neurons. *International Joint Conference on Neural Networks (IJCNN).*

2. Tae Seung Kang, Arunava Banerjee, (2017) Learning Deterministic Spiking Neuron Feedback Controllers. *International Joint Conference on Neural Networks (IJCNN).*

3. Gokhan Kaya (2016) Signal Coding and Reconstruction through a Framework Which Utilizes Naturally-Inspired Deterministic Spiking Models. *Ph.D Thesis*, University of Florida.

4. Tae Seung Kang (2017) Learning Feedforward and Recurrent Deterministic Spiking Neuron Network Feedback Controllers. *Ph.D Thesis*, University of Florida.

5. Inchul Choi (2018) Multi-Scale Generalized PlaneMatch based Occlusion Detection and Correspondence for Optical Flow. *Ph.D Thesis*, University of Florida.

6. Tae Seung Kang, Arunava Banerjee (2018) Learning Feedforward and Recurrent Deterministic Spiking Neuron Network Feedback Controllers. *arXiv:1708.02603.*

7. Arunava Banerjee (2019) An Optimization framework for Nonspiking Neuronal Networks and Aided Discovery of a Model for the Elementary Motion Detector. *BioRxiv doi: https://doi.org/10.1101/666149.* (under review).

8. Anik Chattopadhyay, Arunava Banerjee (2019) Signal Coding and Perfect Reconstruction using Spike Trains. *arXiv:1906.00092.* (under review).

9. Michael Kummer, Arunava Banerjee (2020) Spike-Triggered Descent. *arXiv:2005.05572.* (under review).

References

[1] Arunava Banerjee. Learning precise spike train–to–spike train transformations in multi-layer feedforward neuronal networks. *Neural computation*, 28(5):826–848, 2016.

[2] H. B. Barlow and W. R. Levick. The mechanism of directionally selective units in rabbit's retina. *Journal of Physiology*, 178:477–504, 1965.

[3] Horace B Barlow. Possible principles underlying the transformations of sensory messages. *Sensory Communication, Ed W.Rosenblith*, pages 217–234, 1961.

[4] Rudy Behnia, Damon A. Clark, Adam G. Carter, Thomas R. Clandinin, and Claude Desplan. Processing properties of on and off pathways for drosophila motion detection. *Nature*, 512:427—430, 2014.

[5] William Bialek, Fred Rieke, RR De Ruyter Van Steveninck, and David Warland. Reading a neural code. *Science*, 252(5014):1854–1857, 1991.

[6] Alexander Borst, Juergen Haag, and Dierk F. Reiff. Fly motion vision. *Annual Review of Neuroscience*, 33:49–70, 2010.

[7] Stephen Boyd and Leon Chua. Fading memory and the problem of approximating nonlinear operators with volterra series. *IEEE Transactions on circuits and systems*, 32(11):1150–1161, 1985.

[8] Julian Jakob Bussgang. Crosscorrelation functions of amplitude-distorted gaussian signals. 1952.

[9] Evan C Smith and Michael Lewicki. Efficient auditory coding. *Nature*, 439:978–82, Mar 2006.

[10] EJ Chichilnisky. A simple white noise analysis of neuronal light responses. *Network: Computation in Neural Systems*, 12(2):199–213, 2001.

[11] Dmitri B. Chklovskii and Daniel Soudry. Neuronal spike generation mechanism as an oversampling, noise-shaping a-to-d converter. In F. Pereira, C. J. C. Burges, L. Bottou, and K. Q. Weinberger, editors, *Advances in Neural Information Processing Systems 25*, pages 503–511. 2012.

[12] R Christopher deCharms and Michael M Merzenich. Primary cortical representation of sounds by the coordination of action-potential timing. *Nature*, 381(6583):610, 1996.

[13] Damon A. Clark, Limor Bursztyn, Mark A. Horowitz, Mark J. Schnitzer, and Thomas R. Clandinin. Defining the computational structure of the motion detector in drosophila. *Neuron*, 70:1165—1177, 2011.

[14] Ingrid Daubechies and Ron DeVore. Approximating a bandlimited function using very coarsely quantized data: A family of stable sigma-delta modulators of arbitrary order. *Annals of Mathematics*, 158(2):679–710, 2003.

[15] Egbert De Boer and Paul Kuyper. Triggered correlation. *IEEE Transactions on Biomedical Engineering*, (3):169–179, 1968.

[16] Hugo G Eyherabide, Ariel Rokem, Andreas VM Herz, and Inés Samengo. Burst firing is a neural code in an insect auditory system. *Frontiers in Computational Neuroscience*, 2:3, 2008.

[17] Hugo G Eyherabide, Ariel Rokem, Andreas VM Herz, and Inés Samengo. Bursts generate a non-reducible spike-pattern code. *Frontiers in Neuroscience*, 3:2, 2009.

[18] P. Földiák. Forming sparse representations by local anti-hebbian learning. *Biological Cybernetics*, 64(2):165–170, Dec 1990.

[19] Eduardo Fonseca, Manoj Plakal, Frederic Font, Daniel P. W. Ellis, Xavier Favory, Jordi Pons, and Xavier Serra. General-purpose tagging of freesound audio with audioset labels: Task description, dataset, and baseline, 2018.

[20] J. F. Gemmeke, D. P. W. Ellis, D. Freedman, A. Jansen, W. Lawrence, R. C. Moore, M. Plakal, and M. Ritter. Audio set: An ontology and human-labeled dataset for audio events. In *2017 IEEE International Conference on Acoustics, Speech and Signal Processing (ICASSP)*, pages 776–780, 2017.

[21] Wulfram Gerstner, J Leo Van Hemmen, and Jack D Cowan. What matters in neuronal locking? *Neural computation*, 8(8):1653–1676, 1996.

[22] Daniel Graham and David Field. Sparse coding in the neocortex. *Evolution of Nervous Systems*, 3:181–187, 2007.

[23] B. Hassenstein and W. Reichardt. Systemtheoretische analyse der zeit-, reihenfolgen- und vorzeichenauswertung bei der bewegungsperzeption des rüsselkäfers chlorophanus. *Zeitschrift Für Naturforschung*, 11:513–524, 1956.

[24] Alan L Hodgkin and Andrew F Huxley. A quantitative description of membrane current and its application to conduction and excitation in nerve. *The Journal of physiology*, 117(4):500–544, 1952.

[25] M. Joesch, B. Schnell, S. V. Raghu, D. F. Reiff, and A. Borst. On and off pathways in drosophila motion vision. *Nature*, 468:300—304, 2010.

[26] Roland S Johansson and Ingvars Birznieks. First spikes in ensembles of human tactile afferents code complex spatial fingertip events. *Nature neuroscience*, 7(2):170–177, 2004.

[27] Mikko Juusola, Andrew S. French, Raimo O. Uusitalo, and Matti Weckström. Information processing by graded-potential transmission through tonically active synapses. *Trends Neurosci.*, 19(7):292–297, 1996.

[28] Michael S. Lewicki. Efficient coding of natural sounds. *Nature Neuroscience*, 5:356–363, Mar 2002.

[29] S. G. Mallat and Zhifeng Zhang. Matching pursuits with time-frequency dictionaries. *IEEE Transactions on Signal Processing*, 41(12):3397–3415, 1993.

[30] Panos Z Marmarelis and Ken-Ichi Naka. White-noise analysis of a neuron chain: an application of the wiener theory. *Science*, 175(4027):1276–1278, 1972.

[31] Ian A. Meinertzhagen and S. D. O'Neil. Synaptic organization of columnar elements in the lamina of the wild type in drosophila melanogaster. *J Comp Neurol*, 305(2):232–263., 1991.

[32] Markus Meister, Leon Lagnado, Denis A Baylor, et al. Concerted signaling by retinal ganglion cells. *Science*, pages 1207–1207, 1995.

[33] Ilya Nemenman, Geoffrey D Lewen, William Bialek, and Rob R de Ruyter van Steveninck. Neural coding of natural stimuli: information at sub-millisecond resolution. *PLoS computational biology*, 4(3):e1000025, 2008.

[34] Sergio Neuenschwander and Wolf Singer. Long-range synchronization of oscillatory light responses in the cat retina and lateral geniculate nucleus. *Nature*, 379(6567):728, 1996.

[35] David J. Olshausen, Bruno A.and Field. Emergence of simple-cell receptive field properties by learning a sparse code for natural images. *Nature*, 381:607–609, Jun 1996.

[36] R. Patterson, Ian Nimmo-Smith, J. Holdsworth, and P. Rice. An efficient auditory filterbank based on the gammatone function. 01 1988.

[37] Fred Rieke, David Warland, R de Ruyter van Steveninck, and William Bialek. Spikes: Exploring the neural code mit press. *Cambridge MA*, 1997.

[38] A. Rokem, S. Watzl, T. Gollisch, M. Stemmler, A.V.M. Herz, and I. Samengo. Recordings from grasshopper (locusta migratoria) auditory receptor cells., 2009.

[39] Ariel Rokem, Sebastian Watzl, Tim Gollisch, Martin Stemmler, Andreas VM Herz, and Inés Samengo. Spike-timing precision underlies the coding efficiency of auditory receptor neurons. *Journal of Neurophysiology*, 95(4):2541–2552, 2006.

[40] Odelia Schwartz, Jonathan W Pillow, Nicole C Rust, and Eero P Simoncelli. Spike-triggered neural characterization. *Journal of vision*, 6(4):13–13, 2006.

[41] Samuel Shapero, Mengchen Zhu, Jennifer Hasler, and Christopher Rozell. Optimal sparse approximation with integrate and fire neurons. *International journal of neural systems*, 24:1440001, 08 2014.

[42] Kazunori Shinomiya, Gary Huang, Zhiyuan Lu, Toufiq Parag, C. Shan Xu, Roxanne Aniceto, Namra Ansari, Natasha Cheatham, Shirley Lauchie, Erika Neace, Omotara Ogundeyi, Christopher Ordish, David Peel, Aya Shinomiya, Claire Smith, Satoko Takemura, Iris Talebi, Patricia K. Rivlin, Aljoscha Nern, Louis K. Scheffer, Stephen M. Plaza, and Ian A. Meinertzhagen. Comparisons between the on- and off- edge motion pathways in the drosophila brain. *eLife*, 8:e40025, 2019.

[43] Malcolm Slaney. An efficient implementation of the patterson-holdsworth auditory filter bank. 11 2000.

[44] Shin Ya Takemura, Aljoscha Nern, Dmitri B. Chklovskii, Louis K. Scheffer, Gerald M. Rubin, and Ian A. Meinertzhagen. The comprehensive connectome of a neural substrate for 'on' motion detection in drosophila. *eLife*, 6:e24394, 2017.

[45] John C. Tuthill, Aljoscha Nern, Stephen L. Holtz, Gerald M. Rubin, and Michael B. Reiser. Contributions of the 12 neuron classes in the fly lamina to motion vision. *Neuron*, 79(10):128–140, 2013.

[46] Michael Wehr and Gilles Laurent. Odour encoding by temporal sequences of firing in oscillating neural assemblies. *Nature*, 384(6605):162, 1996.

[47] Norbert Wiener. Nonlinear problems in random theory. *Nonlinear Problems in Random Theory, by Norbert Wiener, pp. 142. ISBN 0-262-73012-X. Cambridge, Massachusetts, USA: The MIT Press, August 1966.(Paper)*, page 142, 1966.

[48] Zhihao Zheng, J Scott Lauritzen, Eric Perlman, Camenzind G Robinson, Matthew Nichols, Daniel Milkie, Omar Torrens, John Price, Corey B Fisher, Nadiya Sharifi, et al. A complete electron microscopy volume of the brain of adult drosophila melanogaster. *Cell*, 174(3):730–743, 2018.

[49] Joel Zylberberg, Jason Timothy Murphy, and Michael Robert DeWeese. A sparse coding model with synaptically local plasticity and spiking neurons can account for the diverse shapes of v1 simple cell receptive fields. *PLOS Computational Biology*, 7(10):1–12, 10 2011.